Santoso, Imam; Riihimäki, Markus; Sibarani, David; Taskinen, Pekka; Hupa, Leena; Paek, Min Kyu; Lindberg, Daniel

Impact of recently discovered sodium calcium silicate solutions on the phase diagrams of relevance for glass-ceramics in the Na_2O-CaO-SiO_2 system

Published in:
Journal of the European Ceramic Society

DOI:
10.1016/j.jeurceramsoc.2022.01.010

Published: 01/05/2022

Document Version
Publisher's PDF, also known as Version of record

Journal of the European Ceramic Society 42 (2022) 2449–2463

Contents lists available at ScienceDirect

Journal of the European Ceramic Society

journal homepage: www.elsevier.com/locate/jeurceramsoc

Impact of recently discovered sodium calcium silicate solutions on the phase diagrams of relevance for glass-ceramics in the Na_2O-CaO-SiO_2 system

Imam Santoso [a,*], Markus Riihimäki [b], David Sibarani [c], Pekka Taskinen [c], Leena Hupa [d], Min-Kyu Paek [c], Daniel Lindberg [c,*]

[a] Department of Metallurgical Engineering, Institut Teknologi Bandung, Bandung, Indonesia
[b] Faculty of Technology, Environmental and Chemical Engineering, Oulu University, Oulu, Finland
[c] School of Chemical Engineering, Aalto University, Espoo, Finland
[d] Faculty of Science and Engineering, Åbo Akademi University, Turku, Finland

ARTICLE INFO

Keywords:
Glass
Ceramics
Slags
Thermodynamics
Phase diagram

ABSTRACT

Although phase relations in the Na_2O-CaO-SiO_2 system are vital to melting and thermal treatments in glass and glass-ceramics industries, the available data for thermodynamic modeling are mostly based on reports published in 1920s and 1950s. The present investigation verifies the formation of solid solutions of Na_2CaSiO_4 and $Na_2Ca_2Si_2O_7$ which have previously assumed to be stoichiometric compounds. The impact of these solid solutions on the features of the phase diagram were investigated using the equilibration-quenching-EDS/EPMA technique. The data were reported as liquidus projections and in isothermal sections within the temperature range of 1000 and 1400 °C. Ten primary phase fields were identified, namely SiO_2, $Na_2Ca_3Si_6O_{16}$, combeite, $Na_4CaSi_3O_9$ss, $CaSiO_3$, Na_2CaSiO_4ss, $Na_2Ca_2Si_2O_7$ss, $Na_2Ca_6Si_4O_{15}$, $Ca_3Si_2O_7$ and Ca_2SiO_4. In addition, some novel liquidus data and invariants points were examined in more detail. The fundamental data obtained can be employed for the thermodynamic reassessment of the Na_2O-CaO-SiO_2 system. The present study also discusses the findings and their impact on melting and annealing processes during the manufacture of glass and glass-ceramics.

1. Introduction

Soda-lime-silica is the most important glass family in daily life because 90 % of the manufactured conventional glasses in the world belong to the Na_2O-CaO-SiO_2 system [1]. The Na_2O-CaO-SiO_2 glass system is also vital in many medical applications, including several compositions used for tissue engineering and drug delivery [2,3]. Understanding the behavior of the Na_2O-CaO-SiO_2 system, e.g., the phase relations among those present at high temperatures, is therefore crucial for manufacturing these glasses and ceramics. One tool to help manufacturers in the essential task of successfully predicting the melting range of a particular mixture and the crystalline phases formed during any subsequent heat treatment is the detailed understanding of the phase diagram Na_2O-CaO-SiO. However, the data used to construct this diagram is based on the classic papers by Kracek [4] and Morey and Bowen [5] in 1925 and further developed by Segnit [6], as resumed in the book of Phase Diagram for Ceramist [7]. For the metallurgical industries, the system is vital for slags as Na_2O could significantly decrease their melting point and increase a slag's capacity to remove impurities [8]. For the incineration technology to process the Municipal Solid Waste (MSW), the system is important as the slag, accounted for 85 % by weight formed in the bottom of the reactors as the solid residue, contains considerable amounts of Na_2O, CaO and SiO_2 [9,10]

Morey and Bowen [5] experimentally investigated the phase relations of liquid with solid phases in the Na_2O-CaO-SiO_2 system by using the melting-quenching technique. The samples were prepared from the mixture of $CaCO_3$, Na_2CO_3 and SiO_2 heated using platinum crucible to form a glass which was used for the phase equilibria measurement. The glass composition was analyzed before the equilibration to measure phase relations. The quenched phases were examined by using optical microscope. They reported SiO_2, $CaSiO_3$, Na_2SiO_3, $Na_2Si_2O_5$, $Na_2Ca_2Si_3O_9$, $Na_8Ca_3Si_5O_{17}$, $Na_4CaSi_3O_9$, and $Na_2Ca_3Si_6O_{16}$ primary phase fields. Then, Segnit [6] used the same experimental method used by Morey and Bowen [5] extended the study to the area containing less

* Corresponding authors.
E-mail addresses: imam.santoso@metallurgy.itb.ac.id (I. Santoso), daniel.k.lindberg@aalto.fi (D. Lindberg).

https://doi.org/10.1016/j.jeurceramsoc.2022.01.010
Received 13 September 2021; Received in revised form 3 January 2022; Accepted 4 January 2022
Available online 6 January 2022

Table 1
Chemicals used in the present Investigation.

No	Chemical	purity, wt-%	Supplier
1	SiO_2	99.9	Umicore
2	CaO	99.9	Sigma Aldrich
3	Na_2CO_3	99.9	Sigma Aldrich
4	Na_2SiO_3	96	Alfa Aesar

SiO_2 and reported a new compound of $Na_8Ca_3Si_5O_{17}$ and measured liquidus data in the new primary phase fields $Na_8Ca_3Si_5O_{17}$, Ca_2SiO_4, $Ca_2Si_2O_7$, Na_2CaSiO_4, and $Na_2Ca_2Si_2O_7$. He [6] experienced difficulty at high temperatures due to soda volatilization. Later, Sahid and Glasser [11] revised the diagram after finding new crystalline phases of $Na_2CaSi_5O_{12}$ and $Na_6Si_8O_{19}$ and measured their liquidus points employing the same methods as Morey and Bowen [5].

However, the chemical composition measurements of the glasses reported by Morey and Bowen [5], Segnit [7], Sahid and Glasser [11] were undertaken before the re-melting in the equilibration process during which liquidus of the mixtures was measured. The phases in the quenched samples were examined using optical microscopy. As Na_2O is a volatile component, losing Na_2O to the atmosphere during the melting is likely to change the concentration of Na_2O compared to the initial mixture. With regard to this limitation, post-equilibrium chemical analysis of the sample by employing the Equilibration-Quenching-EPMA method may be the solution [12]. Zhang et al. [13] also employed this method, although they quenched their samples in a nitrogen atmosphere that gives a slow quenching rate. As indicated in their results, the quenched liquid phases were not homogenous because they turned into microcrystalline phases during the quenching. This change proves that the liquid properties stable at high temperatures cannot be preserved to room temperature as the melt's composition might alter during the quenching process. Therefore, it is difficult to indicate the composition of the phases formed and phase relations from their results [13].

The existence of two solid solutions in the ternary system was reported by Moir and Glasser [14] when they reexamined the stability of combeite ($Na_2Ca_2Si_3O_9$) and $Na_4CaSi_3O_9$ compounds characterized by using XRD analysis for the samples synthesized using Morey and Bowen's techniques [5]. They showed that combeite was not a stoichiometric compound of $Na_2Ca_2Si_3O_9$, neither $Na_4CaSi_3O_9$. These compounds form solid solutions existing in the pseudo-binary Na_2SiO_3-$CaSiO_3$ system. Combeite has a compositional range of Na_2SiO_3 between 28.5 and 53.5 mol-%, whereas the $Na_4CaSi_3O_9$ has a much smaller range. They also reported solid solution of β-$CaSiO_3$ that can dissolve up to 2 mol-% Na_2SiO_3. Fedorov and Brodkina [15] outlined a solid solution of β-Ca_2SiO_4 in the pseudo-binary Ca_2SiO_4 and Na_2CaSiO_4. β-Ca_2SiO_4 was found to dissolve up to 10 wt-% Na_2CaSiO_4 at 1300 °C at which the sample was annealed and then characterized by XRD method. Toropov and Arakelyan [16] identified two new compounds in the Ca_2SiO_4 and Na_2CaSiO_4 system, hexagonal $Na_4Ca_8Si_5O_{20}$ and $Na_4Ca_4Si_3O_{12}$. However, according to Fedorov and Brodkina [15], $Na_4Ca_8Si_5O_{20}$ is actually a β-Ca_2SiO_4 solid solution and $Na_4Ca_4Si_3O_{12}$ does not exist.

In terms of thermodynamic modeling, Thermo-Calc [18] was employed by L. Zhang et al. [17] to assess the Na_2O-CaO-SiO_2 system. The sub-lattice model was used to describe the Gibbs energy of liquid. Later, Z. Zhang et al. [19] assessed the system using a modified associated species model to evaluate the Gibbs energy of the liquid phase and employing FactSage using FToxid database [20] for the calculation. Some disagreements were obvious between the results in these two works by Z. Zhang et al. and L. Zhang et al. For example, in the diagram produced by L. Zhang et al. [17], the pseudo-binary Na_2SiO_3-$CaSiO_3$ section was much more complicated than the one presented by Z. Zhang et al. [19]. It is because the computed quasi-binary diagram by L. Zhang et al. [17] did not indicate the stability of the Ca_2SiO_4, $Na_2Si_6O_7$, and $Na_2Ca_2Si_3O_9$ compounds. However, these compounds were stable in the computed quasi-binary diagram by Z. Zhang et al. [19].

Kahlenberg et al. [21] recently reported the $Na_2Ca_6Si_4O_{15}$ compound. Its liquidus data have not been available in the literature. Therefore, the inclusion of this compound in the thermodynamic assessment of the Na_2O-CaO-SiO_2 system will affect the computed phase diagrams. They [21] synthesized the compound by using Na_2CO_3-$CaCO_3$-SiO_2 placed in a platinum container and heated 1300 °C and then quenched. The sample was characterized by using EPMA to measure chemical compositions and by employing X-ray diffractometer to collect crystallographic data. The existence of some compounds, such as $Na_8Ca_3Si_5O_{17}$, $Na_2Ca_3Si_2O_8$ and $Na_2CaSi_5O_{12}$, was questioned [22] as they cannot be reproduced experimentally by using the crystallization approach and solid-state syntheses.

It is obvious that there is a lack of reliable experimental liquidus data for mixtures with higher Na_2O contents. The omission of liquidus data for the newly reported crystals is evident. Disagreement among the authors [17,19] is also apparent. To conclude the above analysis, to better understand the formation of suggested additional crystalline phases and their liquidus, experimental reinvestigation of the system Na_2O-CaO-SiO_2 is required. In the present study, the Equilibration-Quenching-EPMA/EDS method was employed to study the Na_2O-CaO-SiO_2 system over a wide composition range of SiO_2 from 33.33 to 84.2 mol-% and Na_2O up to 47.5 mol-% between 1000 and 1400 °C. The primary phase fields were explored to derive the saturation boundary lines of the compounds. Furthermore, liquidus with double saturation was also studied to obtain the univariant lines, which are the boundary lines between two adjacent primary phase fields. Comparison of the data obtained in the present work to previous research, as well as the computed phase diagram was undertaken. The results are discussed in relation to the manufacturing of the glass.

2. Methods

When investigating the equilibrium properties of phases occurring at high temperatures, the phases must be preserved by rapid cooling in a cold medium. Then, the composition and homogeneity of the phases can be examined under a microanalyzer. The liquid must be preserved as a glassy phase, and also the solid phase composition must be maintained. In the present investigation, the sample preparation challenges, were met by utilizing the Equilibration-Quenching-EPMA/EDS technique.

2.1. Sample preparation

The high purity chemicals presented in Table 1 were used for the preparation of the initial mixtures. The chemicals were weighed and mixed carefully using an agate mortar and pestle, then pressed to form a 0.15 g pellet. It was important to know the degree of Na_2O volatilization during the equilibration process; thus, the excess amount of Na_2O in the samples was specified accurately to obtain the targeted phase relations. Failing to take into account the volatilization would result in unwanted phase equilibria as the evaporation changes the location of the tie lines and the proportions between equilibrium phases.

Na_2O concentration in the mixture was adjusted to form a liquid saturated with one or several crystalline phases. Otherwise, if the mixture formed upon quenching only amorphous phase(s), the liquidus boundaries would not be revealed. For this purpose, the diagram computed by FactSage using FToxid database [20] and MTDATA [23] using MTOX database [24] were used as the initial guidance for the mixtures.

2.2. Equilibration process

The pellets were placed in a platinum container and held by a platinum wire in the center of the hot zone of the reaction tube with 30 mm inner diameter, made from impervious recrystallized alumina, inside a furnace (Nabertherm RHTV 120-150/18, heated with $MoSi_2$ heating

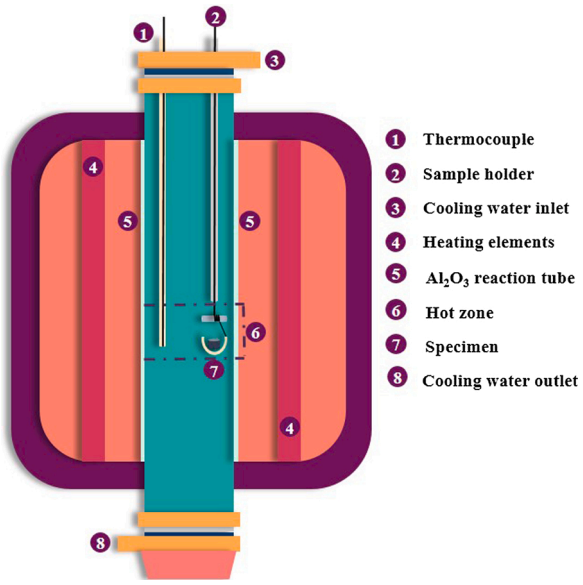

Fig. 1. Furnace arrangement.

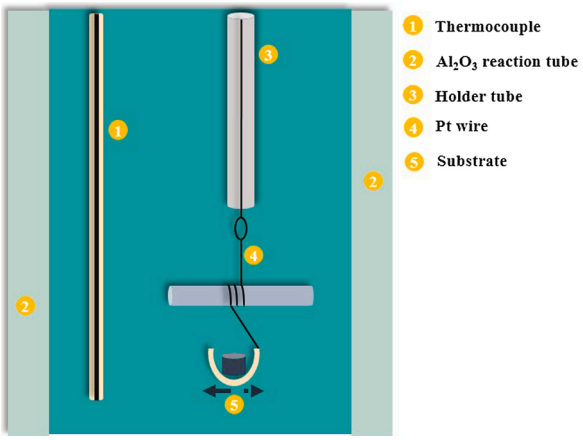

Fig. 2. Sample container design.

Table 2
Comparison between EDS analysis results and stoichiometric values of the formed crystalline compounds.

Analysis	$Na_2Ca_6Si_4O_{15}$ composition (mol-%)			$Na_2Ca_3Si_6O_{16}$ composition (mol-%)		
	Na_2O	CaO	SiO_2	Na_2O	CaO	SiO_2
True stoichiometric value	9.1	54.6	36.4	10.0	30.0	60.0
EDS	9.2	54.8	36.0	10.2	29.5	60.3

Table 3
Comparison between EDS and EPMA analysis results of the solid and liquid phases.

Analysis	Solid composition (mol-%)			Liquid composition (mol-%)		
	Na_2O	CaO	SiO_2	Na_2O	CaO	SiO_2
EPMA	26.0	40.2	33.8	27.8	38.7	33.6
EDS	26.5	39.7	33.8	28.2	38.2	33.6

element, Germany) to equilibrate the samples. The arrangement of the furnace and the design of the Pt crucible can be seen in Figs. 1 and 2, respectively. The top of the reaction tube was equipped with two holes for the thermocouple sheath and one for a mini tube to protect the wire. A calibrated S-type thermocouple of Pt/Pt-10 wt-% Rh (Johnson-Matthey, UK) was placed close to the samples and connected to a multimeter (Keithley, USA), which was linked to a computer program (NI LabView) to continuously measure and document the temperature of the samples every 5 s. Temperature uncertainty of ±2 °C was achieved. The bottom of the reaction tube was open to the air.

2.3. Equilibrium confirmation

Equilibrium attainment can be ensured from three different criteria: time, the direction of approach, and homogeneity. An equilibrium has been reached if samples heated at different equilibration times but at the same temperature locate on the same liquidus line. Therefore, samples in the present investigation were equilibrated at different holding times, and the results showed that the sample could reach equilibrium after 1 h or 2 days depending on temperature and the specific type of equilibria. The second criterion means that the same equilibrium state must be reachable either by heating the sample directly to the targeted temperature or by pre-melting, i.e., overheating the sample and then cooling it down to the targeted temperature. Also, the criterion is satisfied if different compounds used as the initial mixture can produce the same equilibrium condition. In the present investigation, mixtures of Na_2CO_3-CaO-SiO_2 or Na_2SiO_3-CaO-SiO_2 were employed (used as the main mixtures) to ensure that the solid phase in the final state was formed by chemical reactions, not from the unreacted oxides in the initial mixture.

The equilibrium state can be attained as well from the direction of the right side with lower Na_2O content and from the left side with higher Na_2O content. For example, the equilibrium state of $Na_2Ca_2Si_2O_7$ solid solution ($Na_2Ca_2Si_2O_7$ss) can be reached from the $Na_2Ca_2Si_3O_9$ solid solution (combeite) or the Na_2CaSiO_4 solid solution (Na_2CaSiO_4ss). From the thermodynamic point of view, if the equilibria of liquid-$Na_2Ca_2Si_2O_7$ss exist, the equilibria of liquid-$Na_2Ca_2Si_2O_7$ss-Na_2CaSiO_4ss and equilibria of liquid-$Na_2Ca_2Si_2O_7$ss-combeite must exist as well. According to the third criterion, no concentration gradient in any phase is allowed. Hence, the liquidus microanalyses were undertaken at multiple locations to ensure an equal concentration throughout the phases.

2.4. Quenching

After the equilibrium was achieved, the sample was dropped to cooled water by pulling upward the platinum wire that holds the sample. The quenched samples were then dried immediately using hot flash air and mounted in epoxy resin. The sample was polished by using a dry technique, carbon coated and sent for chemical analysis. There was no difficulty to obtain samples which contained glassy phase.

2.5. Phase examination

The samples were analyzed using EPMA (JXA-8530 F Plus Hyper Probe, Jeol, Japan) at Center for Material Analysis, University of Oulu and EDS (ThermoFisher Scientific UltraDry, USA) installed in SEM (Tescan Mira3, Tescan, Czech Republic) at Aalto University. Optimized instrument parameters were needed because of matrix modification resulted from the sodium ion migration in the sample during measurement. For the EPMA measurement 15 kV, 15 μm and 10 s of accelerating voltage, beam diameter, measuring time, respectively, were selected to measure the glass/amorphous phases. For the EDS measurement, area analysis of 100-200 μm^2, 15 kV accelerating voltage and 420 nA current were employed. Tugtupite ($Na_4BeAlSi_4O_{12}Cl$), calcite ($CaCO_3$) and quartz (SiO_2) minerals were used as Na, Ca and Si standards, respectively. ZAF correction was used for EPMA and EDS analyses. A comparison of results between EDS measured values and true stoichiometric values are presented in Table 2. Table 3 shows a comparison of the result obtained with EDS and EPMA analyses of the Na_2CaSiO_4ss compound and its amorphous phase representing the liquid phase at the high

Table 4
Phase compositions measured by EDS analysis.

Sample #	Temperature	Equilibration time (h)	Phases	Composition (mol-%)		
				Na_2O	CaO	SiO_2
NCS-146	1000	55.5	Liquid	15.7	11.7	72.6
			$Na_2Ca_3Si_6O_{16}$	10.2	29.5	60.3
NCS-147	1000	55.5	Liquid	17.5	11.9	70.6
			$Na_2Ca_3Si_6O_{16}$	10.2	29.8	60
NCS-148	1000	55.5	Liquid	20.1	12.6	67.4
			$Na_2Ca_3Si_6O_{16}$	10.4	29.7	59.9
			Combeite	16.8	33.3	49.9
NCS-150	1000	55.5	Liquid	24	9.9	66
			Combeite	19.1	31	49.9
NCS-151	1000	55.5	Liquid	28.2	7.5	64.3
			Combeite	22	28.3	49.6
NCS-152	1000	43	Liquid	40.2	2.9	57
			$Na_4CaSi_3O_9$ss	32.1	17.1	50.7
NCS-155	1000	43	Liquid	36	4.3	59.7
			$Na_4CaSi_3O_9$ss	32.3	17.5	50.2
			Combeite	24.5	25.6	49.9
NCS-157	1000	43	Liquid	33.9	5	61.1
			Combeite	24.2	26.2	49.6
NCS-158	1000	43	Liquid	26.1	8.6	65.3
			Combeite	20.7	29.5	49.8
NCS-159	1000	43	Liquid	31.7	5.8	62.5
			Combeite	23.4	27	49.7
NCS-160	1000	43	Liquid	17.8	5.9	76.3
			SiO_2	0	0	100
NCS-162	1000	43	Liquid	36.8	4.2	59.1
			$Na_4CaSi_3O_9$ss	32.6	17.3	50.1
			Combeite	24.6	25.5	49.9
NCS-163	1000	43	Liquid	15.4	10.1	74.5
			SiO_2	0	0	100
NCS-338	1000	30	Liquid	21.6	11.3	67.1
			Combeite	17.7	32.4	49.9
NCS-341	1000	30	Liquid	20.4	11.9	67.7
			Combeite	17	33	50
NCS-183	1100	6	Liquid	40.6	15.8	43.6
			Na_2CaSiO_4ss	30.7	35.5	33.8
NCS-190	1100	7	Liquid	37.5	18.6	43.9
			$Na_2Ca_2Si_2O_7$ss	20.3	40.2	39.5
			Na_2CaSiO_4ss	29.3	37	33.7
NCS-192	1100	7	Liquid	37.1	17.5	45.4
			$Na_2Ca_2Si_2O_7$ss	20	40.4	39.6
NCS-193	1100	7	Liquid	36.7	17.4	45.9
			$Na_2Ca_2Si_2O_7$ss	20.3	40.2	39.5
			$Na_4CaSi_3O_9$ss	32.3	18	49.7
NCS-196	1100	8	Liquid	36.1	7.6	56.3
			$Na_4CaSi_3O_9$ss	32.1	18	49.9
			Combeite	24.4	25.8	49.8
NCS-199	1100	8	Liquid	29.1	9.4	61.6
			Combeite	21.3	29	49.7
NCS-200	1100	24	Liquid	22.1	14.8	63.1
			Combeite	18.4	31.8	49.8
NCS-204	1100	24	Liquid	19.8	16.2	64
			Combeite	16.9	33.2	49.9
NCS-205	1100	24	Liquid	17.4	17.9	64.7
			$CaSiO_3$	0	50.5	49.5
			Combeite	15.1	34.9	50
NCS-207	1100	24	Liquid	16.3	16.4	67.4
			$CaSiO_3$	0	50.1	49.9
NCS-209	1100	24	Liquid	14.6	15.3	70.2
			$CaSiO_3$	0	50.1	49.9
NCS-214	1100	24	Liquid	12.1	14.2	73.7
			SiO_2	0	0	100
			$CaSiO_3$	0	49.9	50.1
NCS-216	1100	24	Liquid	14.6	8.8	76.7
			SiO_2	0	0	100
NCS-217	1100	24	Liquid	17	4	79
			SiO_2	0	0	100
NCS-8	1200	75	Liquid	13.1	6.4	80.6
			SiO_2	0	0	100
NCS-10	1200	75	Liquid	8.3	18.7	73
			SiO_2	0	0	100
			$CaSiO_3$	0	50.3	49.7
NCS-12	1200	75	Liquid	10.5	20.8	68.7
			$CaSiO_3$	0	50.2	49.8

(*continued on next page*)

Table 4 (*continued*)

Sample #	Temperature	Equilibration time (h)	Phases	Composition (mol-%)		
				Na_2O	CaO	SiO_2
NCS-13	1200	44	Liquid	10.7	20.7	68.6
			$CaSiO_3$	0	50.3	49.7
NCS-14	1200	44	Liquid	11.3	21.8	66.9
			$CaSiO_3$	0	50.4	49.6
NCS-15	1200	44	Liquid	13.3	23.4	63.3
			$CaSiO_3$	0	50.3	49.7
NCS-16	1200	44	Liquid	13.6	25.4	61
			$CaSiO_3$	0	50.2	49.8
NCS-19	1200	72	Liquid	19	22.8	58.1
			Combeite	16.6	33.4	50
NCS-28	1200	68	Liquid	25.5	18.2	56.3
			Combeite	19.8	30.5	49.7
NCS-81	1200	6	Liquid	34	22.9	43.1
			Na_2CaSiO_4ss	27	39.3	33.6
NCS-85	1200	6	Liquid	31	17	52.1
			Combeite	22.1	28.2	49.7
NCS-99	1200	6	Liquid	30	25.3	44.7
			$Na_2Ca_2Si_2O_7$ss	18.6	41.6	39.8
NCS-102	1200	6	Liquid	31.2	25.9	42.9
			$Na_2Ca_2Si_2O_7$ss	20.1	40.7	39.1
			Na_2CaSiO_4ss	26.5	39.7	33.8
NCS-107	1200	46	Liquid	26.7	27.2	46.1
			$Na_2Ca_2Si_2O_7$ss	17.3	43.1	39.6
			Combeite	21.5	28.9	49.6
NCS-115	1200	22	Liquid	20.4	21	58.6
			Combeite	16.7	33.6	49.7
NCS-116	1200	22	Liquid	20.4	21	58.6
			Combeite	16.8	33.5	49.8
NCS-117	1200	22	Liquid	23.1	19.3	57.6
			Combeite	18.1	32.3	49.7
NCS-120	1200	22	Liquid	15.1	26.3	58.5
			Combeite	13.8	36.3	49.9
			$CaSiO_3$	0	50.5	49.5
NCS-166	1200	21	Liquid	29.6	22.6	47.9
			Combeite	22.8	27.5	49.6
NCS-167	1200	21	Liquid	30.6	19.6	49.8
			Combeite	23.4	27	49.6
NCS-285	1200	1	Liquid	47.5	12.7	39.8
			Na_2CaSiO_4ss	32.9	33.9	33.1
NCS-290	1200	2	Liquid	42.5	15.7	41.8
			Na_2CaSiO_4ss	31.1	35.6	33.3
NCS-294	1200	2	Liquid	40.2	18	41.8
			Na_2CaSiO_4ss	30	36.7	33.3
NCS-345	1200	5	Liquid	37.2	20.2	42.7
			Na_2CaSiO_4ss	28.9	37.6	33.5
NCS-36	1300	24	Liquid	5.4	24.1	70.5
			SiO_2	0	0	100
			$CaSiO_3$	0	50.2	49.8
NCS-40	1300	24	Liquid	9.7	29.7	60.6
			$CaSiO_3$	0	50.3	49.7
NCS-42	1300	24	Liquid	7.7	26.9	65.4
			$CaSiO_3$	0	50.4	49.5
NCS-43	1300	24	Liquid	7.4	48.1	44.5
			Ca_2SiO_4ss	0.3	66.4	33.3
NCS-45	1300	24	Liquid	9.7	42.4	47.9
			$CaSiO_3$	0	50.2	49.8
NCS-48	1300	24	Liquid	8.4	47.4	44.2
			$Na_2Ca_6Si_4O_{15}$	7.7	56.2	36.2
NCS-50	1300	24	Liquid	14.4	40.7	44.9
			$Na_2Ca_6Si_4O_{15}$	8.4	55.7	35.8
NCS-137	1300	4.5	Liquid	16	39.2	44.8
			$Na_2Ca_6Si_4O_{15}$	8.7	55.1	36.2
NCS-170	1300	5	Liquid	10.7	9.1	80.2
			SiO_2	0	0	100
NCS-171	1300	5	Liquid	8.9	13.7	77.3
			SiO_2	0	0	100
NCS-172	1300	5	Liquid	11.9	36.8	51.3
			$CaSiO_3$	0	50.5	49.5
NCS-179	1300	13	Liquid	11.7	43.3	45
			$Na_2Ca_6Si_4O_{15}$	8.6	55.1	36.4
NCS-300	1300	12	Liquid	7.9	46.7	45.4
			$CaSiO_3$	0	50.2	49.9
			$Ca_3Si_2O_7$	0	59.9	40.1
NCS-315	1300	1	Liquid	30.1	27.8	42.1

(*continued on next page*)

Table 4 (*continued*)

Sample #	Temperature	Equilibration time (h)	Phases	Composition (mol-%)		
				Na_2O	CaO	SiO_2
			Na_2CaSiO_4ss	25.8	41	33.2
			Liquid	26.4	31.8	41.8
NCS-350	1300	1	$Na_2Ca_6Si_4O_{15}$	9.2	54.8	36
			Na_2CaSiO_4ss	24.2	42.6	33.2
NCS-362-a	1300	1	Liquid	37.1	21	41.9
			Na_2CaSiO_4ss	29.1	37.6	33.3
NCS-362	1300	1	Liquid	33.7	24.8	41.5
			Na_2CaSiO_4ss	27.9	38.7	33.4
NCS-55	1400	20.5	Liquid	8.1	7.7	84.2
			SiO_2	0	0	100
NCS-58	1400	20.5	Liquid	5.4	19.1	75.5
			SiO_2	0	0	100
NCS-63	1400	28	Liquid	2.7	33.9	63.4
			$CaSiO_3$	0	50.4	49.6
NCS-65	1400	28	Liquid	6.2	36.8	57
			$CaSiO_3$	0	50.4	49.6
NCS-69	1400	28	Liquid	9.7	47.3	43
			Ca_2SiO_4ss	2.1	64.3	33.6
NCS-73	1400	4.5	Liquid	16.8	41	42.2
			$Na_2Ca_6Si_4O_{15}$	8.8	55	36.2
NCS-74	1400	4.5	Liquid	14.2	43.3	42.5
			$Na_2Ca_6Si_4O_{15}$	8.5	55.5	36
			Liquid	3.6	52.5	43.9
NCS-305	1400	6	$CaSiO_3$	0	50.3	49.7
			$Ca_3Si_2O_7$	0	60	40
			Liquid	25.3	33.8	40.8
NCS-328	1400	1	Na_2CaSiO_4ss	23.4	43.4	33.2
			Liquid	22.5	36.8	40.8
NCS-358	1400	1	$Na_2Ca_6Si_4O_{15}$	9.2	54.5	36.4
			Na_2CaSiO_4ss	22.5	44.3	33.3

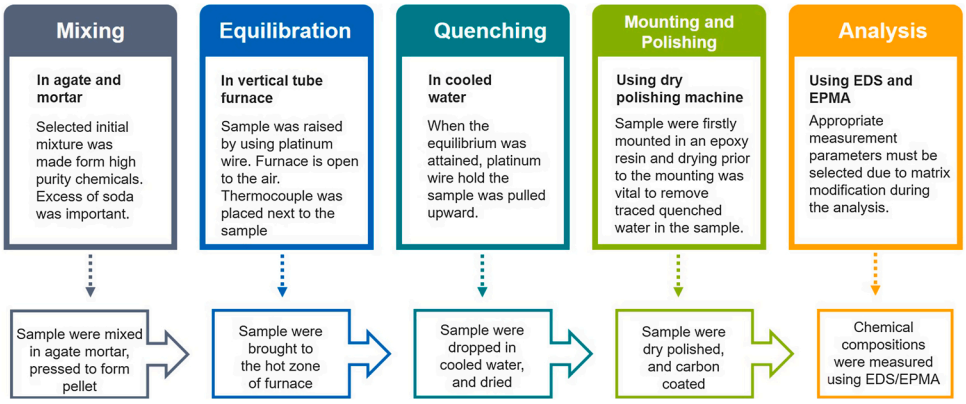

Fig. 3. Method employed in the present investigation.

temperature equilibrium condition.

It can be seen in Table 2 that the EDS results are in very close agreement with the theoretical values. They are also in good agreement with the EPMA results, as indicated in Table 3. The maximum uncertainties obtained were less than 1 mol-%. In the present study, EDS analysis results of liquid phase are presented together with the results of solid phase analysis, in Table 4. Therefore, the analysis accuracy of each amorphous phase, i.e., liquid phase at the high temperature, also can be checked from the results of the respective solid phase. The method is summarized in Fig. 3.

2.6. Computational phase diagram

The computed phase diagrams presented were calculated by FactSage 7.3. using FToxid database [20] and MTDATA [23] using MTOX database, version 8.2 [24]. The obtained phase diagrams were then compared with the experimental data.

3. Result and discussion

The compositional analyses of the amorphous (liquid) and solid phases using EDS are reported in Table 4. In the present study, 10 primary phase fields were obtained since altogether 10 solid compounds were found to exist in equilibrium with the liquid phase and verified in the quenched samples. These were the phase fields of SiO_2, $Na_2Ca_3Si_6O_{16}$, combeite ($Na_2Ca_2Si_3O_9$), $Na_4CaSi_3O_9$ss, $CaSiO_3$, Na_2CaSiO_4ss, $Na_2Ca_2Si_2O_7$ss, $Na_2Ca_6Si_4O_{15}$, $Ca_3Si_2O_7$ and Ca_2SiO_4. The micrographs of a liquid saturated with a single and two types of crystals are presented in Figs. 4 and 5 respectively. The detailed relation among the phases obtained is presented as isothermal sections at 1000, 1100, 1200, 1300 and 1400 °C in Figs. 6–10, respectively. In the isothermal sections, this liquid is represented by tie lines connecting the liquid with the solid compound. The liquid phase is graphically presented as liquidus projections in Fig. 11. The solid phases connected by Alkemade lines are reported in Fig. 12. Each primary phase field intersects with the adjacent

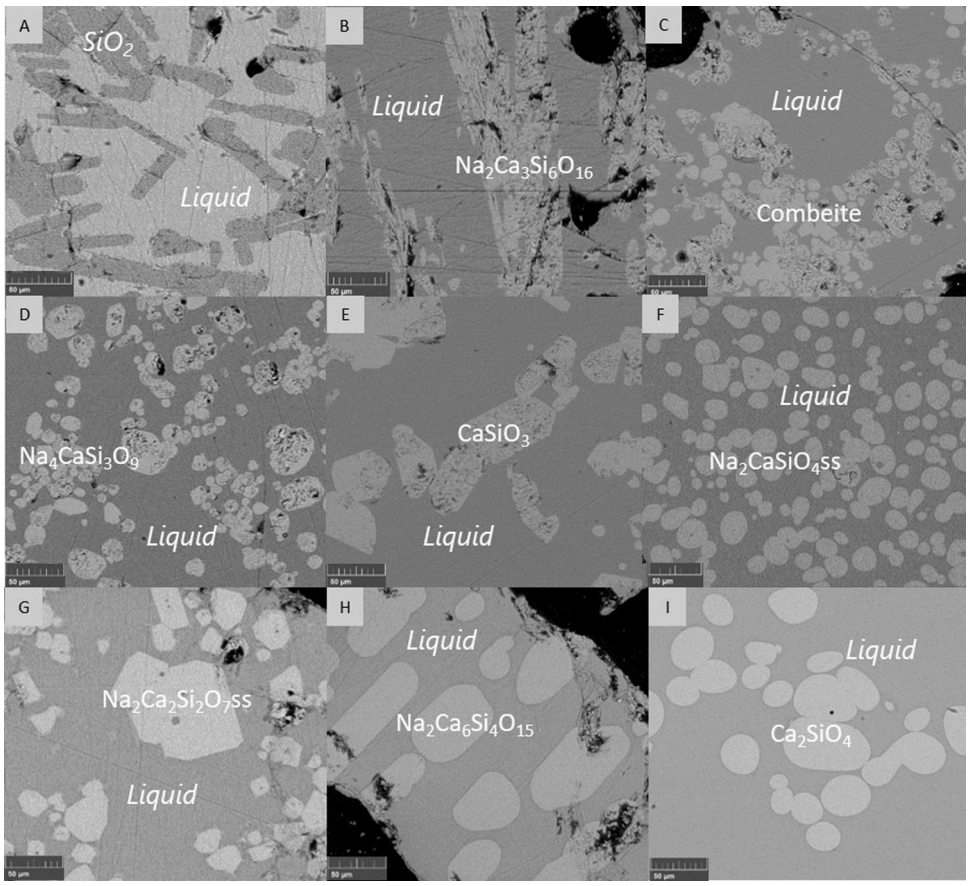

Fig. 4. Backscattered electron micrographs of amorphous phase, i.e. liquid in equilibrium with A. SiO_2; B. $Na_2Ca_3Si_6O_{16}$; C. Combeite; D. $Na_4CaSi_3O_9$ss; E. $CaSiO_3$; F. Na_2CaSiO_4ss; G. $Na_2Ca_2Si_2O_7$ss; H. $Na_2Ca_6Si_4O_{15}$; I. Ca_2SiO_4.

fields along the univariant lines drawn as a solid black line in Fig. 11. The microstructures are represented by the amorphous phase in equilibrium with two solid phases in Fig. 5. In the isothermal sections, this liquid is depicted by the tie triangle connecting the liquid with the two solid compounds.

Altogether, 18 different phase assemblages of the quenched samples were obtained in the present study. These assemblages are collected in Table 5: Liquid + SiO_2, liquid + $Na_2Ca_3Si_6O_{16}$, liquid + combeite, liquid + $Na_4CaSi_3O_9$ss, liquid + $CaSiO_3$, liquid + Na_2CaSiO_4ss, liquid + $Na_2Ca_2Si_2O_7$ss, liquid + $Na_2Ca_6Si_4O_{15}$, liquid + Ca_2SiO_4ss, liquid + SiO_2+$CaSiO_3$, liquid + combeite + $Na_2Ca_3Si_6O_{16}$, liquid + combeite + $Na_4CaSi_3O_9$ss, liquid + combeite + $CaSiO_3$, liquid + combeite + $Na_2Ca_2Si_2O_7$ss, Liquid + Na_2CaSiO_4ss + $Na_2Ca_6Si_4O_{15}$, liquid + $Na_2Ca_2Si_2O_7$ss + $Na_4CaSi_3O_9$ss, liquid + $Na_2Ca_2Si_2O_7$ss + Na_2CaSiO_4ss, and liquid + $CaSiO_3$ + $Ca_3Si_2O_7$.

Comparisons between the experimental data and the calculated phase diagrams by FToxid database [20] are presented in Figs. 13 and 14 as $CaSiO_3$-Na_2SiO_3 and Ca_2SiO_4-Na_4SiO_4 pseudo binary diagrams, respectively. Figs. 15–17 show comparisons between the computed diagrams by FToxid [20] and MTOX databases [24] and the data at 1000, 1200 and 1400 °C, respectively.

3.1. Behavior of Na_2O

The study of the Na_2O evaporation was similar to that used in an earlier study of K_2O [25]. Fig. 18 shows how the tie lines move due to the evaporation of Na_2O. The remaining Na_2O content in the equilibrium phase at a specific temperature depended on the equilibration time and the concentration of Na_2O in the initial mixture. If Na_2O evaporates gradually, the composition will also change gradually following the evaporation line toward the CaO-SiO_2 side, drawn as a dashed line. As shown in Fig. 18, Na_2O concentration in sample NCS-81 decreased from 42.5 mol-% to 31 mol-% after being equilibrated for just 6 h at 1200 °C. However, sample NCS-13 with Na_2O concentration of 10 mol-% in the initial mixture decreased to 7.5 mol-% after 44 h equilibration. Therefore, to obtain a particular final equilibrium assemblage, the specific concentration in the initial mixture must be carefully adjusted.

3.2. Primary phase field of SiO_2

The liquidus point data in SiO_2 primary phase field at 1000 °C are in good agreement with the FToxid database [20] and have slightly lower Na_2O solubility than that calculated with the MTOX database [24] (Fig. 15). The data agree with those reported by Santoso and Taskinen [12], who measured the liquidus data at SiO_2 saturation in the binary Na_2O-SiO_2 system. MTDATA and its MTOX database [24] used the data by Kracek [4] and Morey and Bowen [5] in its assessment where the calculated liquidus line will have higher Na_2O concentration. Thus, the measured liquidus line should be lower in Na_2O content compared to the MTOX database simulation due to some Na_2O evaporation in the experiments by Kracek [4] and Morey and Bowen [5]. The present study reports liquid data in double saturation of SiO_2 and $CaSiO_3$ (Fig. 5A), thus providing data to locate the intersection between the SiO_2 and $CaSiO_3$ primary phase fields. The locations of intersection between SiO_2 and $CaSiO_3$ in the ternary diagram has a higher CaO content than calculated by the FToxid database [20], as indicated in Figs. 16 and 17.

3.3. Primary phase field of $CaSiO_3$

Between 1200 and 1400 °C, liquidus point data at $CaSiO_3$ saturation

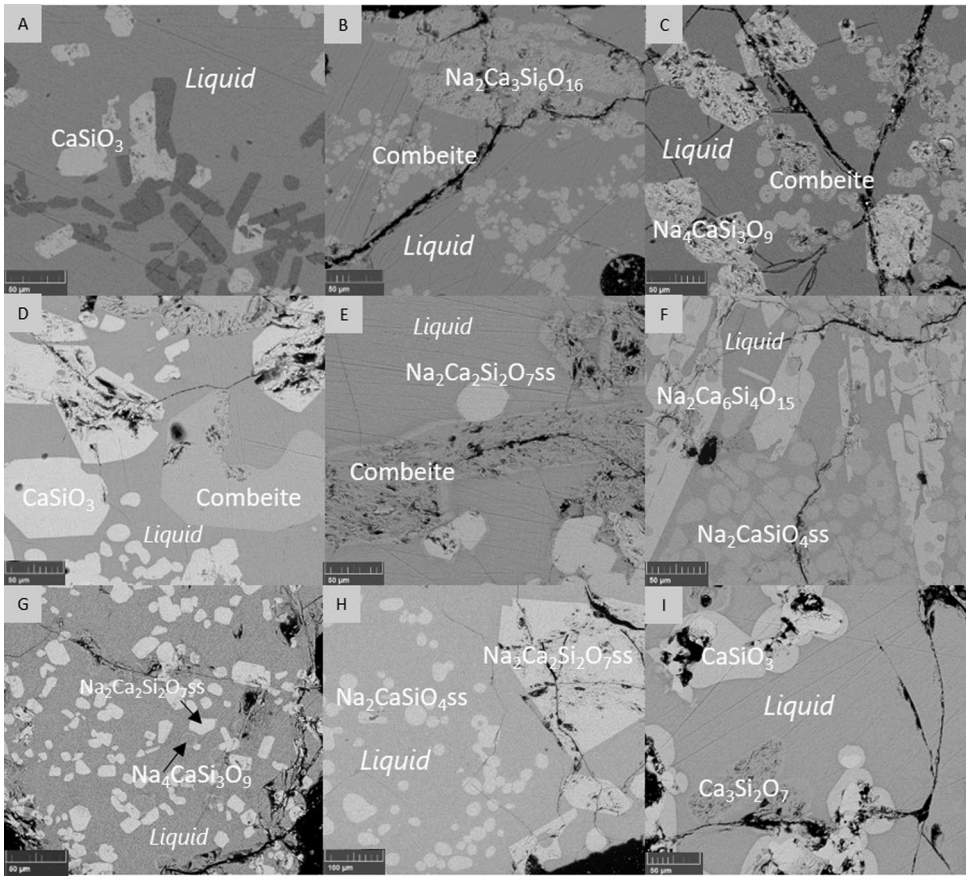

Fig. 5. Backscattered electron micrographs of amorphous phase (liquid) in equilibrium with A. SiO_2 + $CaSiO_3$; B. $Na_2Ca_3Si_6O_{16}$ + Combeite; C. Combeite + $Na_4CaSi_3O_9$ss; D. Combeite + $CaSiO_3$; E. Na_2CaSiO_4ss + $Na_2Ca_6Si_4O_{15}$; F. $Na_2Ca_6Si_4O_{15}$ + Na_2CaSiO_4ss; G. $Na_2Ca_2Si_2O_7$ss + $Na_4CaSi_3O_9$ss; H. Na_2CaSiO_4ss + $Na_2Ca_2Si_2O_7$ss; I. $CaSiO_3$ + $Ca_3Si_2O_7$.

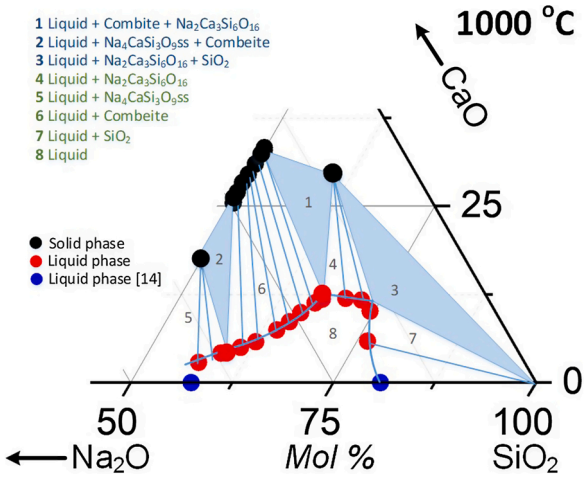

Fig. 6. Isothermal section of the Na_2O-CaO-SiO_2 system at 1000 °C.

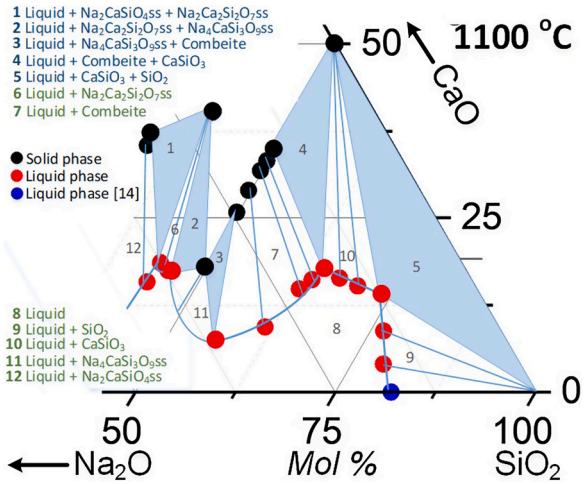

Fig. 7. Isothermal section of the Na_2O-CaO-SiO_2 system at 1100 °C.

are lower in Na_2O content than the liquidus line predicted by FToxid [20] and MTOX databases [24] (Figs. 16 and 17). This difference can be explained by the fact that these two softwares are, again, based on Kracek [4] and Morey and Bowen [5] data. Evaporation of Na_2O should have shifted their data systematically away from the Na_2O corner. According to Moir and Glasser [14], $CaSiO_3$ can dissolve Na_2SiO_3 up to 5 mol-%. However, the present investigation proved that solid $CaSiO_3$ obtained at 1200 and 1300 °C contains only a negligible amount of Na_2O. Liquid compositions at double saturation of $CaSiO_3$ and $Ca_3Si_2O_7$ (Fig. 5I) were obtained at 1300 and 1400 °C, meaning that the intersection location between primary phase fields of $CaSiO_3$ and $Ca_3Si_2O_7$ is known in the ternary diagram.

3.4. Primary phase field of $Ca_3Si_2O_7$

The primary phase field of $Ca_3Si_2O_7$ obtained in the present study is very narrow, as shown in Fig. 11. The width of the liquidus contours is relatively constant at low and high Na_2O concentrations, which agrees

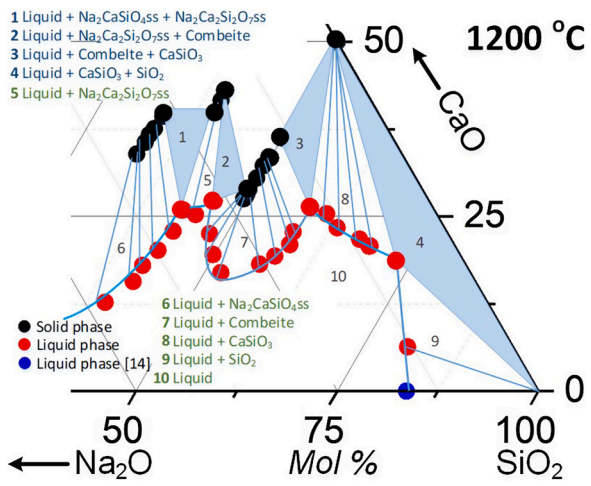

Fig. 8. Isothermal section of the Na_2O-CaO-SiO_2 system at 1200 °C.

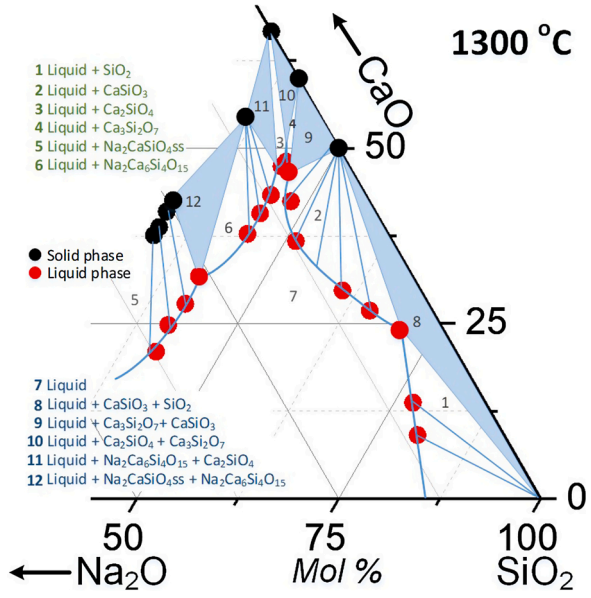

Fig. 9. Isothermal section of the Na_2O-CaO-SiO_2 system at 1300 °C.

with the Segnit [6] report and the values computed with the MTOX database [24]. This kind of feature of the $Ca_3Si_2O_7$ primary phase field was also found to be typical to the $Ca_3Si_2O_7$ primary phase field in the Ka_2O-CaO-SiO_2 system [25]. It differs, however, from the line computed with the FToxid data [20]. The computed field becomes much wider toward the Na_2O-SiO_2 direction. Nevertheless, as shown in Fig. 17, the location of the intersection between the Ca_2SiO_3 and $Ca_3Si_2O_7$ primary phase fields is in good agreement with the predictions of FToxid [20] and MTOX databases [24].

3.5. Primary phase field of Ca_2SiO_4

In the present study, the primary phase field Ca_2SiO_4 was observed at 1300 and 1400 °C. At 1400 °C, Ca_2SiO_4 dissolved 3.1 mol-% Na_4SiO_4 and appears in the pseudo-binary Ca_2SiO_4-Na_4SiO_4 section (Fig. 14). It means that Ca_2SiO_4 formed a solid solution extending to the direction of Na_2CaSiO_4ss, and the maximum solubility of Na_4SiO_4 can be greater than 3.1 mol-% Na_4SiO_4. This is consistent with the results of Fedorov and Brodkina [15]. The primary phase field of Ca_2SiO_4 intersects with the $Na_2Ca_6Si_4O_{15}$ field at 1300 and 1400 °C, as well as the $Ca_3Si_2O_7$ field, whereas FToxid [20] and MTOX databases [24] predict that at

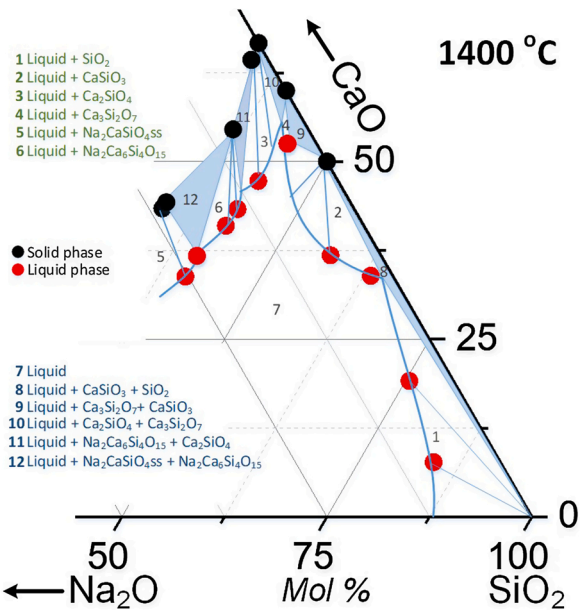

Fig. 10. Isothermal section of the Na_2O-CaO-SiO_2 system at 1400 °C.

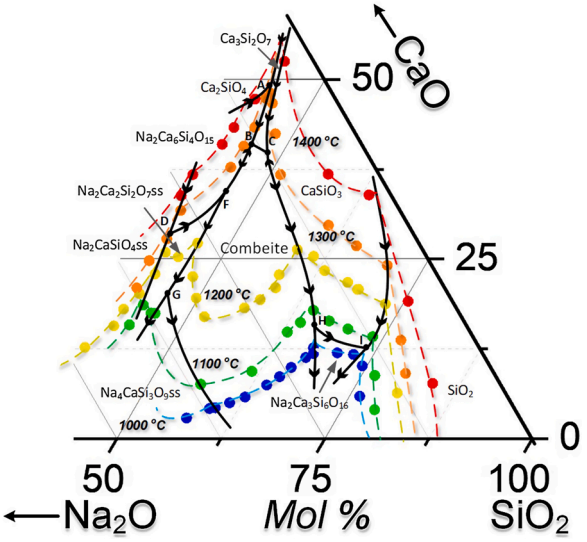

Fig. 11. Liquidus projection and univariant lines (black) of the Na_2O-CaO-SiO_2 system.

1300 and 1400 °C, Ca_2SiO_4 directly crosses the CaO primary phase field. Liquidus at Ca_2SiO_4 saturation obtained in the present investigation is in good agreement with the MTOX database [24] computation.

3.6. Primary phase field of $Na_2Ca_6Si_4O_{15}$

$Na_2Ca_6Si_4O_{15}$ crystals were formed in the sample equilibrated at 1300 and 1400 °C, thus confirming the observations by Kohlenberg [21]. In addition, the present study successfully measured novel liquidus data at $Na_2Ca_6Si_4O_{15}$ saturation. The intersection between the $Na_2Ca_6Si_4O_{15}$ and Na_2CaSiO_4ss primary phase fields between 1300 and 1400 °C was finally confirmed since the liquid phase in the double saturation of $Na_2Ca_6Si_4O_{15}$ and Na_2CaSiO_4ss was verified (Fig. 5F). This compound, $Na_2Ca_6Si_4O_{15}$, is not present in FToxid database [20] and MTOX database [24].

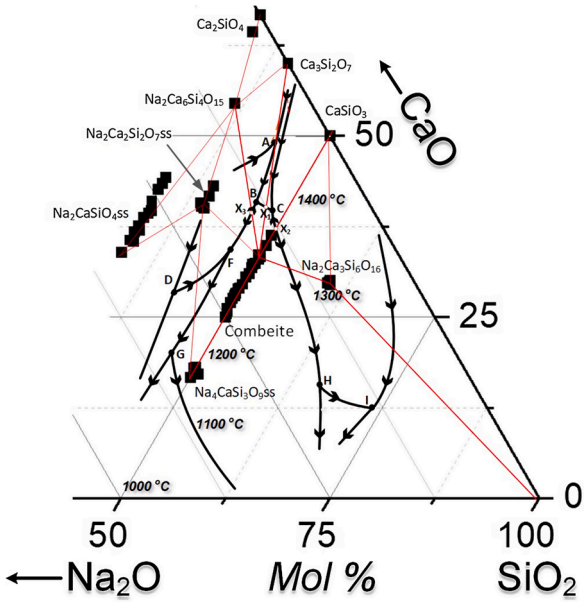

Fig. 12. Invariants points and the Alkemade lines in the Na_2O-CaO-SiO_2 system.

Table 5
Phase assemblages and their microstructures in the present investigation.

No	Phase assemblages	Microstructure
1	Liquid + SiO_2	Fig. 4A
2	Liquid + $Na_2Ca_3Si_6O_{16}$	Fig. 4B
3	Liquid + combeite	Fig. 4C
4	Liquid + $Na_4CaSi_3O_9$ss	Fig. 4D
5	Liquid + $CaSiO_3$	Fig. 4E
6	Liquid + Na_2CaSiO_4ss	Fig. 4F
7	Liquid + $Na_2Ca_2Si_2O_7$ss	Fig. 4G
8	Liquid + $Na_2Ca_6Si_4O_{15}$	Fig. 4H
9	Liquid + Ca_2SiO_4	Fig. 4I
10	Liquid + SiO_2 + $CaSiO_3$	Fig. 5A
11	Liquid + combeite + $Na_2Ca_3Si_6O_{16}$	Fig. 5B
12	Liquid + combeite + $Na_4CaSi_3O_9$ss	Fig. 5C
13	Liquid + combeite + $CaSiO_3$	Fig. 5D
14	Liquid + combeite + $Na_2Ca_2Si_2O_7$ss	Fig. 5E
15	Liquid + Na_2CaSiO_4ss + $Na_2Ca_6Si_4O_{15}$	Fig. 5F
16	Liquid + $Na_2Ca_2Si_2O_7$ss + $Na_4CaSi_3O_9$ss	Fig. 5G
17	Liquid + $Na_2Ca_2Si_2O_7$ss + Na_2CaSiO_4ss	Fig. 5H
18	Liquid + $CaSiO_3$ + $Ca_3Si_2O_7$	Fig. 5I

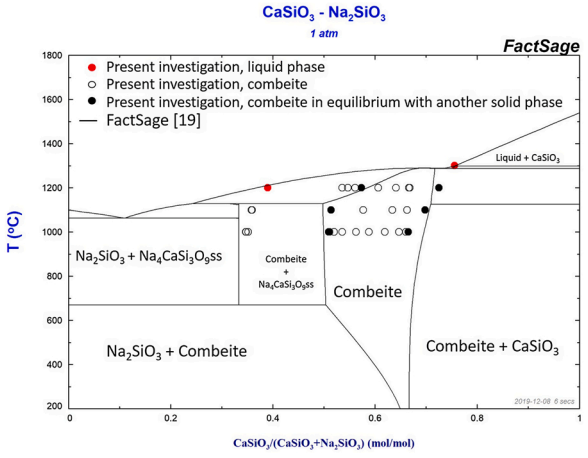

Fig. 13. Computed x,T diagram of the $CaSiO_3$-Na_2SiO_3 section by FToxid database [20].

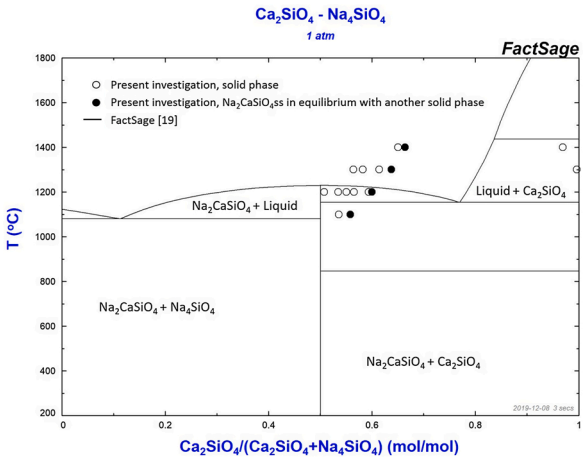

Fig. 14. Computed x, T diagram of the Ca_2SiO_4-Na_4SiO_4 section by FToxid database [20].

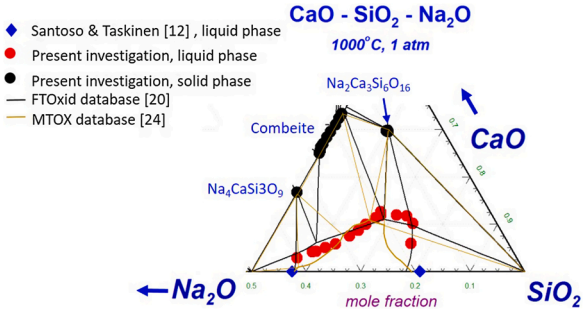

Fig. 15. Computed isothermal sections of the Na_2O-CaO-SiO_2 system at 1000 °C by FToxid and MTOX databases [20,24].

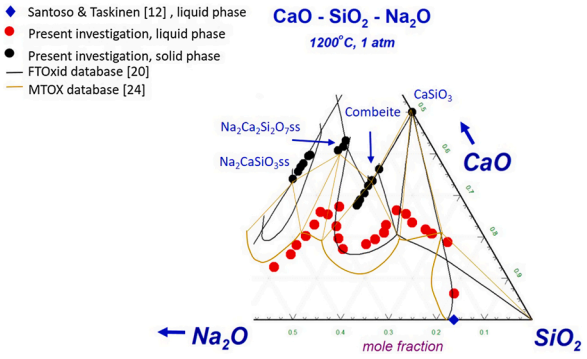

Fig. 16. Computed isothermal sections of the Na_2O-CaO-SiO_2 system at 1200 °C by FToxid and MTOX databases [20,24].

3.7. Primary phase field of combeite

As can be seen in Fig. 13, the combeite phase obtained was located in the pseudo-binary section of Na_2SiO_3 and $CaSiO_3$, ranging for $CaSiO_3$ concentration from 50 to 73 mol-%. The solubility of $CaSiO_3$ in combeite increased with increasing temperature when it in equilibrium with $CaSiO_3$. This observation agrees with the computational phase equilibria of the FToxid database [20] and the data by Moir and Glasser [14]. The liquidus point data obtained in the present investigation are in good agreement with the FToxid database [20] between 1000 and 1200 °C and the MTOX database [24] at 1000 °C (Figs. 15 and 16). MTOX database [24] regards combeite as a stoichiometric compound of $Na_2Ca_2Si_3O_9$. Its computed liquidus line at 1200 °C (Fig. 16) is in poor

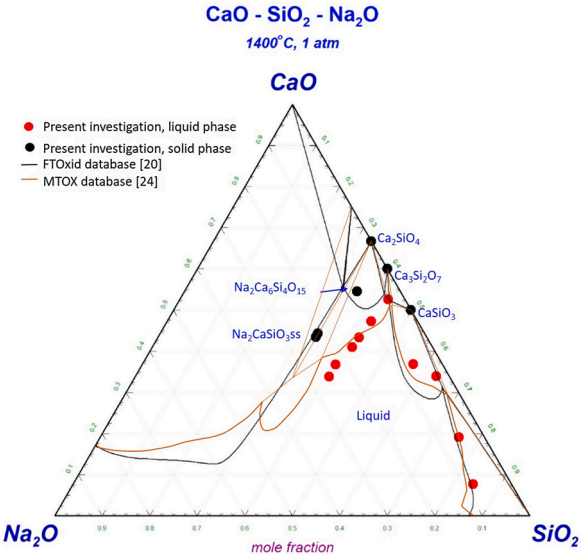

Fig. 17. Computed isothermal sections of the Na_2O-CaO-SiO_2 system at 1400 °C by FToxid and MTOX databases [20,24].

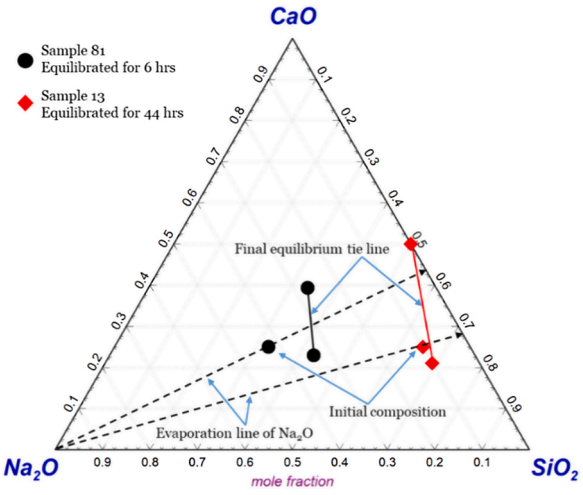

Fig. 18. Evaporation behavior of Na_2O in the Na_2O-CaO-SiO_2 system at 1200 °C.

agreement with the data obtained in the present investigation. Liquid compositions with the double saturation of combeite with $Na_2Ca_3Si_6O_{16}$ (Fig. 5B), $Na_4CaSi_3O_9$ss (Fig. 5C), $CaSiO_3$ (Fig. 5D), and $Na_2Ca_2Si_2O_7$ss (Fig. 5E) were obtained in the present investigation. It means that the locations of the intersections and phase boundaries between combeite with the mentioned primary phase fields are now known in the diagram for the temperature range between 1000 and 1200 °C.

3.8. Primary phase field of $Na_2Ca_2Si_2O_7$ss

The present study indicates that $Na_2Ca_2Si_2O_7$ is not a stoichiometric compound but forms a solid solution, $Na_2Ca_2Si_2O_7$ss, for which the Na_2O concentration in the solution varies from 17.6 to 26.5 mol-% at 1200 °C. This finding provides novel experimental verification showing that $Na_2Ca_2Si_2O_7$ss can form a solid solution. MTOX database [24] considered $Na_2Ca_2Si_2O_7$ as a stoichiometric compound, and the computed liquidus line at 1200 °C is in poor agreement with the data obtained in the present investigation (Fig. 16). FToxid database [20] predicted that $Na_2Ca_2Si_2O_7$ss primary phase field does not exist at 1200

Table 6
Invariant points and the respective phases obtained in present study, pervious investigation [19] and computation [20] by FToxid database.

Point	Phases	Type	Temperature, °C	Liquid Composition, mol-%		
				Na_2O	CaO	SiO_2
A	L + Ca_2SiO_4 = $Ca_3Si_2O_7$+ $Na_2Ca_6Si_4O_{15}$	Peritectic	1295	7.2	49	43.8
B	L = $Ca_3Si_2O_7$+ $Na_2Ca_6Si_4O_{15}$+ Combeite	Eutectic	1285	13.3	41	45.7
C	L = $CaSiO_3$ + Combeite + $Ca_3Si_2O_7$	Eutectic	1280 1400 [19] 1287.7 [20]	11.3	39	49.7
D	L + Na_2CaSiO_4ss = $Na_2Ca_2Si_2O_7$ss + $Na_2Ca_6Si_4O_{15}$	Peritectic	1275	29.7	28.1	42.2
F	L + $Na_2Ca_6Si_4O_{15}$ = $Na_2Ca_2Si_2O_7$ss + Combeite	Peritectic	1220	20.3	34.4	45.7
G	L + Combeite = $Na_2Ca_2Si_2O_7$ss + $Na_4CaSi_3O_9$ss or L + $Na_2Ca_2Si_2O_7$ss = $Na_4CaSi_3O_9$ss + Combeite	Peritectic	1130	34.4	20.3	45.3
H	L + Combeite = $Na_2Ca_3Si_6O_{16}$ + $CaSiO_3$ or L + $CaSiO_3$ = $Na_2Ca_3Si_6O_{16}$ + Combeite	Peritectic	1050 1046.1 [20]	18.8	15.6	66.6
I	L + $CaSiO_3$ = $Na_2Ca_3Si_6O_{16}$ + SiO_2	Peritectic	1030 1027.9 [20]	13.3	12.5	74.2

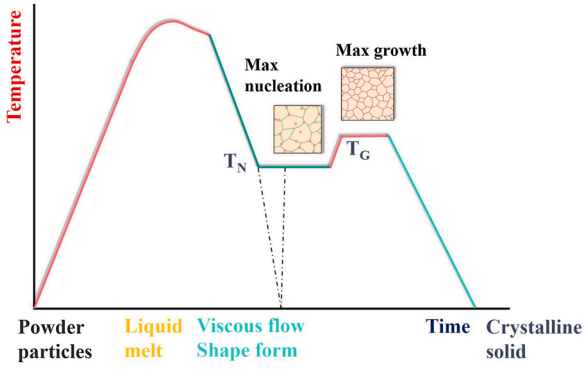

Fig. 19. A schematic diagram showing the steps in the manufacturing of the glass-ceramics [28].

°C (Fig. 16). Liquid at double saturation of $Na_2Ca_2Si_2O_7$ss with Na_2CaSiO_4ss (Fig. 5H) was observed in the present investigation and, thus, the location where these two primary phase fields cross each other can be located in the ternary diagram.

3.9. Primary phase field of Na_2CaSiO_4ss

The details of the location of Na_2CaSiO_4ss in the diagram are presented in Fig. 14. As can be seen in Fig. 14, Na_2CaSiO_4ss is stable in the pseudo-binary Na_4SiO_4 and Ca_2SiO_4 systems. In the ternary diagram, the solid solution is located at a constant SiO_2 concentration of 33.33 mol-%. Between 1100 and 1400 °C, the maximum solubility of Na_4SiO_4 concentration in the solid solution is between 55.8 and 66.4 mol- % and it

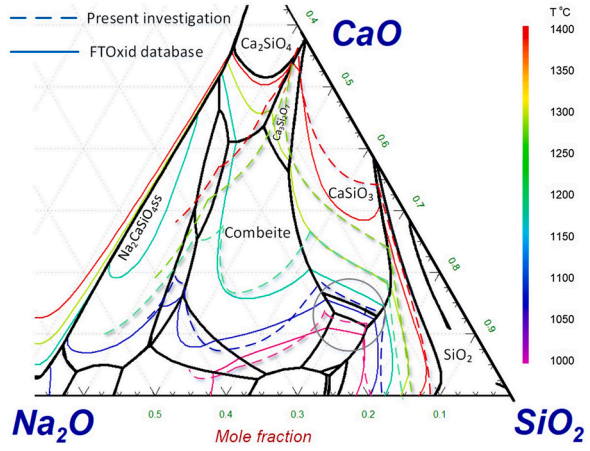

Fig. 20. Liquidus contours and primary phase fields of Na_2O-CaO-SiO_2 system.

increases with increasing temperature. FToxid [20] and MTOX databases [24] regard Na_2CaSiO_4ss as a stoichiometric compound in their assessments. Thus, the computed liquidus at Na_2CaSiO_4 saturation is in poor agreement with the data obtained in the present investigation. As can be seen in Fig. 15, at 1200 °C, the FToxid database [20] predicts that the ternary liquid can contain CaO up to around 53 mol-%. In contrast, according to the present investigation, the maximum CaO concentration in the ternary liquid is only 27.2 mol-%. This can be explained by Na_2CaSiO_4ss being stable within a wide composition range. Thermodynamically, it will reduce the fully liquid region in the ternary diagram. Therefore, the insertion of Na_2CaSiO_4ss to the thermodynamic evaluation of the Na_2O-CaO-SiO_2 system will significantly change the phase assembly of the computed phase diagrams. Accordingly, it is highly recommended that this phase is taken into account as the diagrams in this ternary system are employed in many industrial applications.

3.10. Primary phase field of $Na_4CaSi_3O_9$ss

It can be seen in Fig. 15 that $Na_4CaSi_3O_9$ss is stable at 1000 °C and the liquidus contours obtained in the present investigation are in good agreement with FToxid [20] and MTOX database [24] calculations. $Na_4CaSi_3O_9$ss (Fig. 13) was also observed to form a solid solution in a narrow range of compositions, as also reported by Moir and Glasser [12]. Since the liquidus contour at double saturation of $Na_4CaSi_3O_9$ss and $Na_2Ca_2Si_2O_7$ss (Fig. 5G) was analysed in the present investigation, these solid solutions will be in equilibrium with each other along the univariant lines at different temperatures. However, the FToxid database [20] predicts that the $Na_4CaSi_3O_9$ss primary phase field does not connect to the $Na_2Ca_2Si_2O_7$ss field, but to $Na_8Ca_3Si_5O_{17}$, as reported previously by Segnit [6].

3.11. Primary phase field of $Na_2Ca_3Si_6O_{16}$

It can be seen in Fig. 15 that the liquidus data at $Na_2Ca_3Si_6O_{16}$ saturation obtained at 1000 °C are in good agreement with the computation using the FToxid database [20]. In contrast, the MTOX database [24] predicts the liquid phase domain at $Na_2Ca_3Si_6O_{16}$ saturation to be narrower than the data obtained in the present investigation (Fig. 15).

3.12. Invariant points

By definition, a invariant reaction has zero degrees of freedom in given conditions. Thus, it is almost impossible to determine the exact location of an invariant point at a certain total pressure and temperature in the ternary diagram by experimentation, as the starting mixture already fixes the compositions of the equilibrium phases. Thus, the locations of invariant points were interpolated from temperature and composition data in the ternary diagram. The solid phases analyzed are plotted in Fig. 12 to examine the Alkemade lines [26,27] used to determine the type of the invariant point. The Alkemade lines connectingtwo crystalline compounds were drawn as solid red lines. The lines can only be drawn if the phase fields of the two crystals intersect each other, i.e., they share a common univariant line. Fig. 12 shows the lines of intersection between two adjacent primary phase fields, drawn as black solid lines with arrows indicating the direction of decreasing temperature.

Fig. 12 shows the Alkemade lines of $Na_2Ca_6Si_4O_{15}$-Ca_2SiO_4, $Na_2Ca_6Si_4O_{15}$-Na_2CaSiO_4, Na_2CaSiO_4-$Na_2Ca_2Si_2O_7$, $Na_2Ca_6Si_4O_{15}$-$Na_2Ca_2Si_2O_7$, $Na_2Ca_6Si_4O_{15}$-$Ca_3Si_2O_7$, $CaSiO_3$-$Na_2Ca_3Si_6O_{16}$, SiO_2-$CaSiO_3$, SiO_2-$Na_2Ca_3Si_6O_{16}$, combeite-$Na_2Ca_3Si_6O_{16}$, combeite-$CaSiO_3$, combeite-$Na_2Ca_2Si_2O_7$, combeite -$Na_2Ca_6Si_4O_{15}$, combeite-$Na_4CaSi_3O_9$ss, combeite -$Ca_3Si_2O_7$, $Na_4CaSi_3O_9$-$Na_2Ca_2Si_2O_7$, $Ca_3Si_2O_7$-$CaSiO_3$, and $Ca_3Si_2O_7$-Ca_2SiO_4. $Na_2Ca_2Si_3O_9$ is used to describe combeite because the solid solution composition of combeite will approach to the fixed composition, $Na_2Ca_2Si_3O_9$, upon cooling. This similar approach of composition change of the solid solutions was also applied for Na_2CaSiO_4ss, $Na_2Ca_2Si_2O_7$ss, and $Na_4CaSi_3O_9$ss.

Three Alkemade lines inside the ternary system cross their respective boundary lines of two primary phase fields. Firstly, the boundary between primary phase fields of combeite and $Ca_3Si_2O_7$ crosses the Alkemade line of combeite and $Ca_3Si_2O_7$ at point X_1. Secondly, the Alkemade line of combeite and $Na_2Ca_6Si_4O_{15}$ crosses the boundary between the fields of combeite and $Na_2Ca_6Si_4O_{15}$ at point X_2. Thirdly, the boundary between the primary phase fields of combeite and $CaSiO_3$ crosses the Alkemade line of combeite and $CaSiO_3$ at point X_3. Thus, according to the Alkemade theorem [26,27], points X_1, X_1 and X_3 must be the local maximum points at which temperatures start to decrease in two opposite directions in the lines connecting two adjacent fields. It means that B is a new ternary eutectic of liquid + combeite + $Na_2Ca_6Si_4O_{15}$ + $Ca_3Si_2O_7$ located at the temperature close to 1285 °C. Point C is the ternary eutectic point of liquid + $CaSiO_3$ + combeite + $Ca_3Si_2O_7$ located close to 1280 °C. FToxid database [20] calculated Point C to be 1287.69 °C, although it was predicted as peritectic, not as eutectic point. However, Z. Zhang et al. [19] estimated it to be close to 1400 °C.

Furthermore, the present study suggests the existence of the following peritectic points: (1) liquid + $Ca_3Si_2O_7$ + $Na_2Ca_6Si_4O_{15}$ + Ca_2SiO_4 (Point A) close to 1295 °C; (2) liquid + $Na_2Ca_2Si_2O_7$ss + $Na_2Ca_6Si_4O_{15}$ + Na_2CaSiO_4ss (Point D) at 1275 °C; (3) liquid + $Na_2Ca_2Si_2O_7$ss + $Na_2Ca_6Si_4O_{15}$ + combeite at 1220 °C (Point F) and (4) liquid + $Na_2Ca_2Si_2O_7$ss + $Na_4CaSi_3O_9$ss + combeite (Point G), located 1130 °C.

Peritectic points of liquid + $Na_2Ca_3Si_6O_{16}$ + $CaSiO_3$ + combeite (Point H) at 1050 °C, and liquid + $Na_2Ca_3Si_6O_{16}$ + SiO_2 + $CaSiO_3$ (Point I) at 1030 °C are suggested in the present study. Points H and I were calculated using the FToxid database [20] to be at 1046.11 and 1027.88 °C, respectively. The invariant points and their phases are summarized in Table 6. Furthermore, Figs. 11 and 12 show that the ternary compounds of $Na_2Ca_6Si_4O_{15}$, $Na_2Ca_2Si_2O_7$ss, $Na_4CaSi_3O_9$ss and $Na_2Ca_3Si_6O_{16}$ are located not in their own phase field, meaning that they melt incongruently. As can be seen in Figs. 11 and 12, crystals of $Na_2Ca_6Si_4O_{15}$, $Na_2Ca_2Si_2O_7$ss, $Na_4CaSi_3O_9$ss and $Na_2Ca_3Si_6O_{16}$ are located in the fields of Ca_2SiO_4, $Na_2Ca_6Si_4O_{15}$, combeite and $CaSiO_3$, respectively.

3.13. Implications of the results on the glass and ceramic manufacture

A typical manufacturing process of glass-ceramics is presented schematically in Fig. 19 [28]. It involves melting an oxide mixture in a refractory-lined container to homogenize the melt. The viscous melt is formed to the desired shape, after which the sample is thermally treated to nucleate (T_N, Fig. 19) the desired crystalline phases. Then, the temperature is increased to value providing growth of the crystals (T_G, Fig. 19). Finally, the glass-ceramic sample is annealed to room

temperature. The melting container size can be as large as an Olympic swimming pool if melting, for example, 1600 tons per day. Depending on the original mixture composition, the melting temperatures can be as high as 1600 °C [28] to produce a melt with a low enough viscosity needed to eliminate the gaseous inclusions and dissolve all the crystalline species in the original mixture.

For a glass-ceramic in the ternary system Na_2O-CaO-SiO_2, the ternary invariant point and liquidus temperatures can be employed to estimate the commencement of melting (0% L) and the exact melting point of the mixture (100 % L). The data generated in the present work can also be used to figure out the crystalline phases that form in the thermal treatments of glass-ceramics. However, it should be pointed out that the actual melting temperatures of viscous melts for glasses and glass-ceramics are also affected by the fining and homogenizing criteria.

Fig. 20 shows the liquidus contour compared with the values based on the FTOxid [20] database. The compositions of typical glasses for daily applications e.g., for windows and container glass are also marked in the figure as a large grey circle [28]. Information about the eutectic points is critical for designing the glass since it quantifies the compositions which fully melt at the lowest temperature. This information might be useful when designing compositions with reduced energy and manufacturing costs. Fig. 20 shows that the melting point of a typical glass is actually lower if predicted by the data obtained in the present study than those predicted by FTOxid [20]. The difference is around 50 °C and increases up to 100 °C if the concentration of the mixture located in the $Na_2Ca_3Si_6O_{16}$ primary phase field moves toward primary phase field of $CaSiO_3$ as it showed that liquidus of 1300 °C from present study combined with liquidus of 1400 °C from FTOxid [20]. Present data also can be used to predict the crystal phases and their proposition during annealing more accurately. For example, if the annealing is undertaken in sub-liquidus at certain temperature and as in the field of $CaSiO_3$ the liquidus surfaces obtained in the present study is lower it means that the proposition of crystal to liquid is also smaller than that predicted by FTOxid [20]. Thus, data obtained in present study can be used for process optimization during melting and annealing.

4. Conclusion

Equilibration-quenching-EPMA/EDS method suggested solid solutions of Na_2CaSiO_4 and $Na_2Ca_2Si_2O_7$ in a wide range of compositions in the system Na2O-CaO-SiO2. The impact of the solid solutions on the ternary diagram was investigated together with the primary phase fields of SiO_2, $Na_2Ca_3Si_6O_{16}$, combeite, $Na_4CaSi_3O_9$ss, $CaSiO_3$, Na_2CaSiO_4ss, $Na_2Ca_2Si_2O_7$ss, $Na_2Ca_6Si_4O_{15}$, $Ca_3Si_2O_7$ and Ca_2SiO_4. Novel liquidus data at Na_2CaSiO_4ss, $Na_2Ca_2Si_2O_7$ss, and $Na_2Ca_6Si_4O_{15}$ saturation conditions are reported.

Five new invariant points were suggested based on the data obtained. The liquidus lines at saturation with two different crystalline phases as functions of temperature indicated the locations of the univariant lines as intersections between two adjacent primary phase fields. Comparisons of the data with previous investigations, assessment and computational results by FToxid database [20] databases and MTOX database [24] were also undertaken. Implications of current findings on the manufacturing of the glass and glass ceramics were discussed. The results suggest that Na_2O-CaO-SiO_2 system needs to be reassessed as the many new stable compounds are likely to significantly change many features of the phase properties and the computationally predicted phase equilibria. This study provides fundamental data to be included in the thermodynamic databases.

Data availability

Raw data and other supplementary material are available at the following repository: osf.io/7zpcj.

No data was used for the research described in the article.

Data will be made available on request.

Declaration of Competing Interest

The authors declare that they have no known competing financial interests or personal relationships that could have appeared to influence the work reported in this paper.

Acknowledgements

The study was financially supported by the FLASH project (Predicting the flow behavior of ash mixtures for production of transport biofuels in the circular economy, grant number 280892) within the EnergiX program by the Norwegian Research Council, Norway and also by the Symbiosis of metals production and nature (SYMMET) project of Business Finland. Academy of Finland's RawMatTERS Finland Infrastructure (RAMI) based at Aalto University, VTT Technical Research Centre and Geological Survey of Finland, were applied in this research.

Appendix A

Isoplethal study

To evaluate the univariant line and its direction in the liquid projection diagram of Fig. A1, an isoplethal study was undertaken. In such a study, the reactions and phase relations taking place during cooling of a sample with constant total composition (isopleth) are examined [27]. Furthermore, the study can be used to evaluate how the composition of the solid solution changes during cooling. If the univariant line and the direction of decreasing temperature are correctly constructed, the phase relations obtained during cooling from the isoplethal study will agree with the experimental data.

Fig. A1 shows the line of V- L-P -R-N-G which is the path of the liquid composition changing when mixture V (19.9 mol-% Na_2O, 36.7 mol-% CaO, 43.5 mol-% SiO_2) is cooled from above liquidus to room

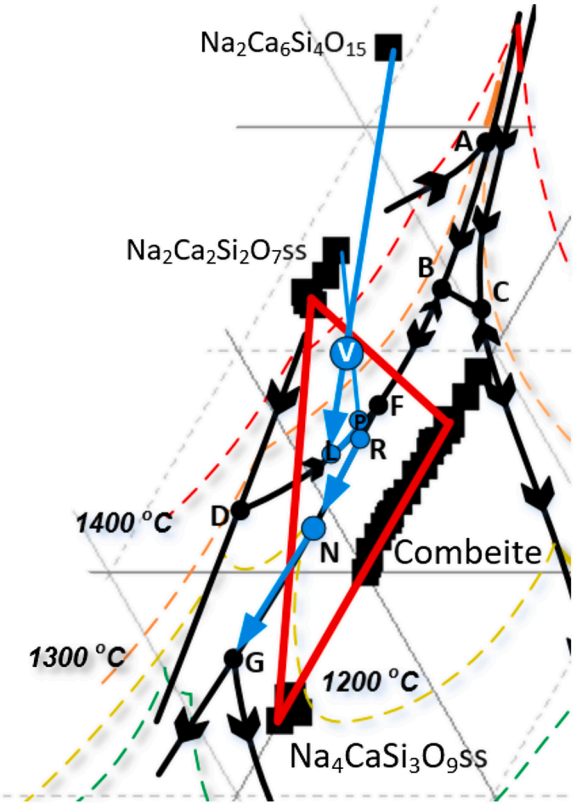

Fig. A1. Isoplethal study and cooling paths of mixtures V on the ternary diagram of Na_2O-CaO-SiO_2.

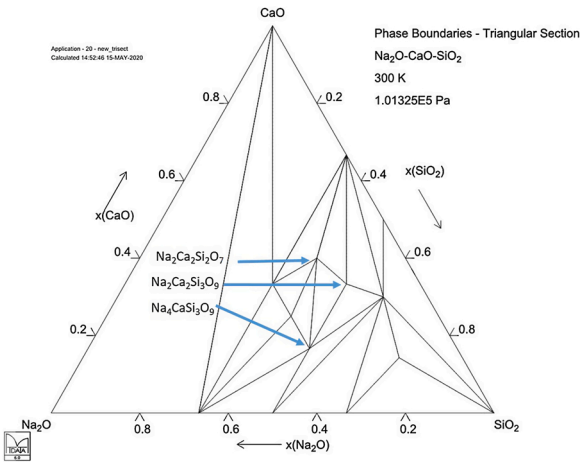

Fig. A2. Isothermal section at room temperature [23,24].

temperature at which all the reactions are completed. When temperature touches the liquidus temperature of 1345 °C, $Na_2Ca_6Si_4O_{15}$ is the first solid to form as V is located in the primary phase field of $Na_2Ca_6Si_4O_{15}$ and the liquidus composition will follow the cooling path of V-L during further cooling. When the cooling path touches the boundary line of D-F at point L, $Na_2Ca_6Si_4O_{15}$ starts to be reabsorbed and a crystal $Na_2Ca_2Si_2O_7$ss starts to form, and the cooling path now follows line of L-P to the direction of peritectic point F. From L to P, $Na_2Ca_6Si_4O_{15}$ is reabsorbed and $Na_2Ca_2Si_2O_7$ss is crystalized, simultaneously. At P, as the tie line $Na_2Ca_2Si_2O_7$ss + liquid crossing V can now directly be drawn, the cooling path moves across the field of $Na_2Ca_2Si_2O_7$ss to point R in the boundary line of F-G without reaching point F. At temperature of P, $Na_2Ca_2Si_2O_7$ss start to form and just below P, $Na_2Ca_6Si_4O_{15}$ disappears. Cooling path now follows the line of R-N on which combeite

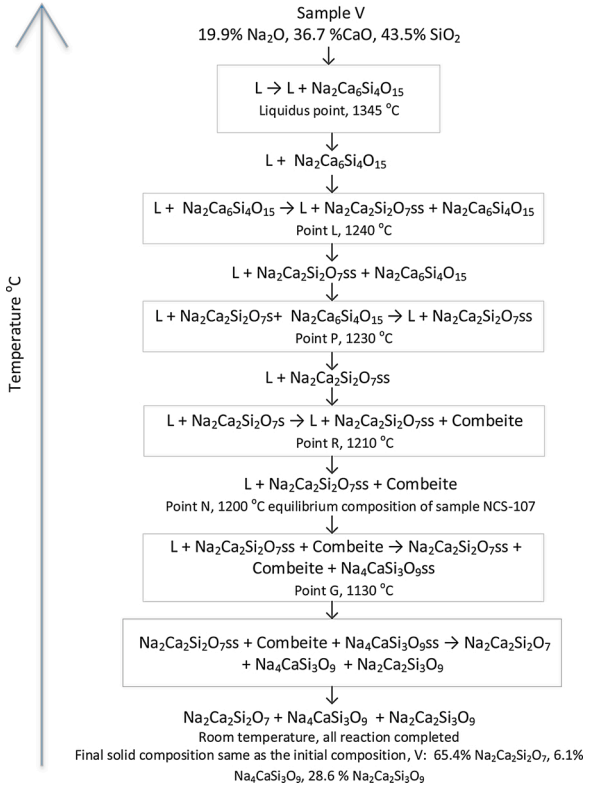

Fig. A3. Phase transformations of sample V during cooling from the melt to 1200 °C and further to room temperature, respectively.

and $Na_2Ca_2Si_2O_7$ss crystalize simultaneously from the liquid. When temperature of 1200 °C is reached, the composition of the liquid is represented by point N and the solid phases are combeite and $Na_2Ca_2Si_2O_7$ss containing 21.5 and 17.3 mol-% Na_2O, respectively (the equilibrium composition of sample NCS-107). They are not stoichiometric compositions of $Na_2Ca_2Si_3O_9$ and $Na_2Ca_2Si_2O_7$.

As the initial mixture of V is located in the Alkemade triangle of $Na_2Ca_2Si_2O_7$-$Na_4CaSi_3O_9$-$Na_2Ca_2Si_3O_9$, according to Alkemade rule, the final assemblage of the solids when all reactions are completed, must be composed of these three stoichiometric crystals with the final composition of V. Thus, during further cooling from 1200 °C, the path will follow the line of N-G and all reactions with liquid will end at the peritectic point of G. At point G, $Na_4CaSi_3O_9$ss start to form, and at a temperature just below G, all liquid vanished. However, the reactions continue during cooling from G to room temperature. The reactions now are in the solid phase and they stop when the three solid solutions have been transformed into stoichiometric compounds. During cooling, from point G to room temperature, combeite composition will shrink to $Na_4CaSi_3O_9$. When it approaches $Na_2Ca_2Si_3O_9$, it will exsolve Na_2O and SiO_2 which are then dissolved by $Na_4CaSi_3O_9$ss and $Na_2Ca_2Si_2O_7$ss forming stoichiometric of $Na_4CaSi_3O_9$ and $Na_2Ca_2Si_2O_7$, respectively. Therefore, when the solidification is completed the final crystal composition is 65.4 mol-% $Na_2Ca_2Si_2O_7$, 6.1 mol-%, $Na_4CaSi_3O_9$, 28.6 mol-% $Na_2Ca_2Si_3O_9$ (point V). This is also indicated by the calculation by MTOX database [24] according to which the $Na_2Ca_2Si_2O_7$-$Na_4CaSi_3O_9$-$Na_2Ca_2Si_3O_9$ triangle exists at low temperatures (Fig. A2) and even already at 1000 °C, as seen in Fig. 15. The reactions and phase relations during cooling of sample Y and V are summarised in Fig. A3.

References

[1] D.W. Oxtoby, H.P. Gillis, L.J. Butler, Principles of Modern Chemistry, Cengage learning, Boston, the United Stated of America, 2015.
[2] E. Leonardi, G. Ciapetti, N. Baldini, G. Novajra, E. Verné, F. Baino, C. Vitale-Brovarone, Response of human bone marrow stromal cells to a resorbable P_2O_5–SiO_2–CaO–MgO–Na_2O–K_2O phosphate glass ceramic for tissue engineering applications, Acta Biomater. 6 (2) (2010) 598–606.
[3] P.M. Reddy, R. Lakshmi, F.P. Dass, S. Sasikumar, Synthesis, characterization and formulation of sodium calcium silicate bioceramic for drug delivery applications, Sci. Eng. Compos. Mater. 23 (4) (2016) 375–380.
[4] F.C. Kracek, The system sodium oxide-silica, J. Phys. Chem. 34 (7) (2002) 1583–1598.
[5] G.W. Morey, N.L. Bowen, The ternary system sodium metasilicate-calcium metasilicate-silica, J. Soc. Glass Technol. 9 (3) (1925) 226–264.
[6] E.R. Segnit, Further data on the system Na_2O-CaO-SiO_2, Am. J. Sci. 251 (8) (1953) 586–601.
[7] L.P. Cook, H.F. McMurdie, Phase Diagrams for Ceramists, Vol. VII, The American Ceramic Society, Ohio, the United Stated of America, 1989.
[8] K. Zhang, Y. Zhang, T. Wu, Distribution ratio of sulfur between CaO-SiO_2-Al_2O_3-Na_2O-TiO_2 slag and carbon-saturated iron, Metals 8 (12) (2018) 1068.
[9] J.D. Eusden, T.T. Eighmy, K. Hockert, E. Holland, K. Marsella, Petrogenesis of municipal solid waste combustion bottom ash, Appl. Geochem. 14 (8) (1999) 1073–1091.
[10] Y. Xiao, M. Oorsprong, Y. Yang, J.H.L. Voncken, Vitrification of bottom ash from a municipal solid waste incinerator, Waste Manag. 28 (6) (2008) 1020–1026.
[11] K.A. Shahid, F.P. Glasser, Phase equilibria in glass forming region of system Na_2O-CaO-SiO_2, Phys. Chem. Glasses 12 (2) (1971) 50.
[12] I. Santoso, P. Taskinen, Phase equilibria of the Na_2O–SiO_2 system between 1173 and 1873 K, Can. Metall. Q. 55 (2) (2016) 243–250.
[13] Z. Zhang, Y. Xiao, J. Voncken, Y. Yang, R. Boom, N. Wang, Z. Zou, Phase equilibria in the Na_2O–CaO–SiO_2 system, J. Am. Ceram. Soc. 94 (9) (2011) 3088–3093.
[14] G.K. Moir, F.P. Glasser, Phase equilibria in the system Na_2SiO_3-$CaSiO_3$, Phys. Chem. Glasses 15 (1) (1974) 6–11.
[15] N.F. Fedorov, E.R. Brodkina, Solid solutions in the system 2CaO•SiO_2-K_2O•CaO•SiO_2, Izv. AN SSSR, Neorg. Mater. 3 (1967) 1283–1284.
[16] N.A. Toropov, O.I. Arakelyan, New calcium and sodium orthosilicates, Doklady Akad. Nauk SSSR 72 (1950) 365–368.
[17] L. Zhang, C. Schmetterer, P.J. Masset, Thermodynamic modeling of the CaO-SiO_2-M_2O (M= K, Na) systems, High Temp. Mater. Process. 32 (3) (2013) 223–228.
[18] B. Sundman, B. Jansson, J.O. Andersson, The Thermo-calc databank system, Calphad 9 (2) (1985) 153–190.
[19] Z. Zhang, Y. Xiao, J. Voncken, Y. Yang, R. Boom, N. Wang, Z. Zhou, Thermodynamic assessment of the CaO-Na_2O-SiO_2 slag system, in: The Eight International Conference on Molten Slags, Fluxes and Salts, Jan. 18–21, 2009 in Santiago, Chile. DC-ROM, Ch IMM, Santiago, 2009, pp. 43–50.
[20] C.W. Bale, E. Bélisle, P. Chartrand, S.A. Decterov, G. Eriksson, K. Hack, I.-H. Jung, Y.-B. Kang, J. Melancon, A.D. Pelton, C. Robelin, S. Petersen, FactSage

thermochemical software and databases—Recent developments, Calphad 33 (2) (2009) 295–311.
[21] V. Kahlenberg, M. Maier, On the existence of a high-temperature polymorph of $Na_2Ca_6Si_4O_{15}$—Implications for the phase equilibria in the system Na_2O-CaO-SiO_2, Mineral. Petrol. 110 (6) (2016) 905–915.
[22] V. Kahlenberg, D. Schmidmair, The system Na_2O-CaO-SiO_2: 90 years of research, but do we really know everything?, August, in: Acta Crystallographica A-Foundation and Advances, Vol. 74, 2018, p. E50.
[23] R.H. Davies, A.T. Dinsdale, J.A. Gisby, J.A.J. Robinson, A.M. Martin, MTDATA-thermodynamic and phase equilibrium software from the national physical laboratory, Calphad 26 (2) (2002) 229–271.
[24] J. Gisby, P. Taskinen, J. Pihlasalo, Z. Li, M. Tyrer, J. Pearce, K. Avarmaa, P. Bjorklund, H. Davies, M. Korpi, S. Martin, L. Pesonen, J. Robinson, MTDATA and the prediction of phase equilibria in oxide systems: 30 years of industrial collaboration, Metall. Mater. Trans. B 48 (1) (2017) 91–98.
[25] I. Santoso, P. Taskinen, A. Jokilaakso, M.K. Paek, D. Lindberg, Phase equilibria and liquid phase behavior of the K_2O-CaO-SiO_2 system for entrained flow biomass gasification, Fuel 265 (2020), 116894.
[26] H.G. Lee, Chemical Thermodynamics for Metals and Materials, Imperial College Press, London, 1999, pp. 213–221.
[27] C.G. Bergeron, S.H. Risbud, Introduction to Phase Equilibria in Ceramics, The American Ceramic Society, Ohio, the United Stated of America, 1984, pp. 94–118.
[28] D.W. Richerson, Modern Ceramic Engineering: Properties, Processing, and Use in Design, CRC press, Boca Raton, 2005, pp. 189–408.